Prediction of pressure drop in gas cylinders with vapor extraction at high and low flow rates

Marc Dequesnes, M. Usman Ghani, and Rick Udischas

American Air Liquide
Chicago Research Center
5230 S. East Avenue
Countryside, IL 60525

Electronic specialty gases (ESGs) are used in the manufacturing processes for semiconductors, fiber optics and flat panel displays. Some ESGs are stored in cylinders in the liquid phase under their own vapor pressure. In order to estimate the amount of gas a cylinder can supply at a given flow rate and required pressure, models are needed for the prediction of the pressure drop in cylinders and the downstream distribution lines as vapor is extracted. The approach for modeling the liquid and gas phase contained in the gas cylinder is similar to the one used for modeling storage tanks and propellant tanks, which assumes uniform liquid and gas temperatures. We have recently improved our model to allow non-uniform liquid temperature.

This improvement has been motivated by the observation that modeling results do not always agree with experiments for low flow rates. We attribute these discrepancies to the boiling phenomenon that is associated with the extraction of vapor from the cylinder. It has been demonstrated experimentally that vapor extraction, at high flow rates, is associated with violent boiling. Therefore, it is expected that for high flow rate for extraction, boiling and natural convection will fully mix the liquid leading to a uniform liquid temperature. For low flow rates, the mixing will not be as pronounced, resulting in non-uniformity of the temperature in the liquid phase. The non-uniformity of temperature is characterized by a sub-cooled liquid/gas interface in the cylinder, resulting in a lower delivery pressure than predicted by assuming a uniform temperature.

In practice, low flow extraction is usually associated with low pressure gases such as tungsten hexafluoride and dichlorosilane. The temperature non-uniformity can be corrected by the use of All Vapor Phase (AVP) gas cabinets [Wang-97]. The AVP gas cabinet incorporates a pressure controlled cylinder-bottom heater to more uniformly heat the liquid in the cylinder, thus improving the extraction flow rate.

This paper presents an improved model that takes into account the non-uniformity of temperature in the liquid phase as well as boiling and natural convection within the liquid. The simulation results with the improved model, which compare well with the experimental results, are presented and discussed.

Introduction

Electronic specialty gases (ESGs) are typically stored in cylinders or ton vessels in the liquid phase under their own vapor pressures. A partial list of ESGs that Air Liquide provides include HCl, HF, Cl_2, NH_3, HBr, BCl_3, C_3F_8, WF_6, Halocarbon 21 and Halocarbon 114. When the vapor

is extracted from the cylinder/ton vessel, the temperature of the liquid decreases, unless sufficient amount of energy is provided to compensate for the heat of vaporization associated with the phase change from liquid to gas.

For medium and high-pressure gases the vapor can be extracted from the cylinder at very high flow rates, typically in the range of 10-100 slpm (standard liters per minute). For the low-pressure gases, the extraction of vapor occurs at relatively lower flow rates usually in the range of 1-10 slpm. When extracting vapor from the cylinder, it has been experimentally demonstrated that this extraction is associated with a violent boiling phenomenon when the extraction flow rate is high. Therefore, it is expected that for medium and high-pressure gases, with high flow rate for extraction, the boiling phenomena and natural convection will mix the liquid leading to a uniform liquid temperature, whereas for low-pressure gases at low flowrates the mixing will not be as pronounced. This is inconsistent with the way the liquid phase is currently modeled in gas cylinders, storage tanks and propellant tanks, which assumes uniform liquid and gas temperatures under all situations. The current formulation would generally be valid for medium and high-pressure gases as the mixing is very pronounced when gas is being withdrawn from the cylinder. However, the model would not be valid for low-pressure gases, where little mixing occurs. Furthermore, there is additional evidence of inadequate mixing of low-pressure gases provided by the experiments conducted at our center. In those experiments the cylinder was intermittently shaken to mix the liquid leading to a more uniform temperature. As a result the experimental data and the predicted results, with the uniform liquid temperature assumption, show much closer agreement (see Figure 3). Therefore, a logical improvement of the model is to stratify the liquid phase into many slices vertically along the cylinder in order to account for the fact that the liquid might not be at a uniform temperature.

Model Basics

The model, presented in this paper, is a significantly improved version of a previous model [Jurcik-96] developed at American Air Liquide. The model takes into account heat transfer due to the vaporization of a liquefied ESG as well as heat transfer from ambient to the container and then to ESG. The basic assumptions made in the formulation of this model are as follows:

- The cylinder is assumed to be initially at thermal equilibrium.
- The temperature drop across the cylinder walls is negligible and, therefore, radial temperature variations in the cylinder wall are ignored: only the vertical variations are considered.
- The radial temperature variations in the heel of the cylinder are taken into account, but the vertical temperature profiles in the heel are not calculated.
- The vapor and liquid temperature fields are stratified, i.e., vary only in the vertical direction.
- The amount of vapor withdrawn is compensated by the same amount of liquefied ESG vaporizing into the headspace.

Figure 1 shows various heat fluxes being considered in the formulation of the model as detailed below:

- Heat transfer through the vertical walls of the cylinder, between the surroundings, and the fluid in the cylinder:
  1. Heat transfer between the surroundings and the external wall of the cylinder.
  2. Heat transfer within the wall of the cylinder.
  3. Heat transfer between the internal wall of the cylinder and the liquid.
  4. Heat transfer between the internal wall of the cylinder and the gas.
- Heat transfer through the cylinder heel:
  5. Heat transfer between the surroundings and the cylinder heel.
  6. Heat transfer within the cylinder heel.
  7. Heat transfer between the cylinder heel and the liquid.
  8. Heat transfer between the liquid and the gas in the cylinder.
  9. Heat transfer due to conduction through the cylinder wall.
  10. Heat transfer due to conduction through the cylinder heel.

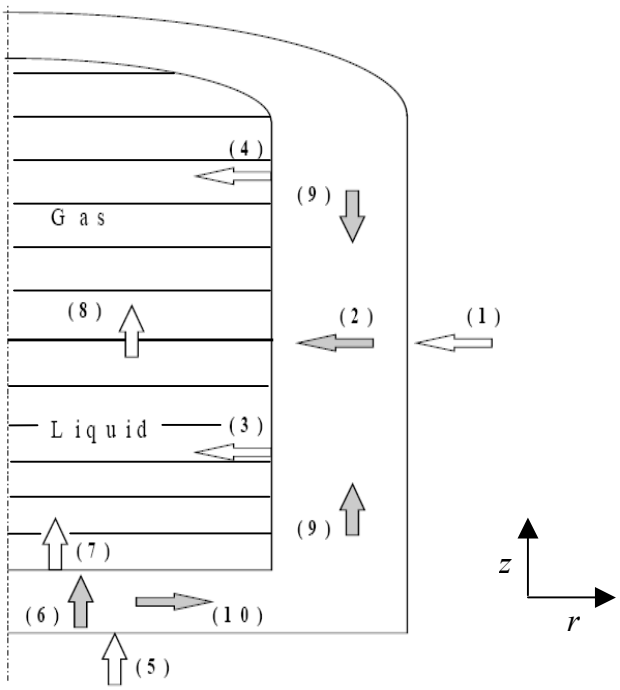

Figure 1. Heat transfer processes as implemented in the model for a cylindrical slice of the cylinder.

Governing Equations

The model is based upon the unsteady mass and energy balances. The differential equations describing these balances are shown below. The corresponding initial and boundary conditions are also shown.

1. Mass balance:

$$\frac{dm_l(t)}{dt} = -\dot{m}(t) \tag{1}$$

with the initial condition

$$m_l(0) = m_{l,0} \tag{1a}$$

2. Liquid energy balance:

The liquid energy balance is based upon the first law of thermodynamics for an open system. In the previous model where the liquid is assumed to be at a uniform temperature, liquid energy balance is given by the following expression:

$$\begin{aligned} m_l(t)\frac{d\hat{U}_l(t)}{dt} = \dot{m}(t)\left[\hat{H}_g(T_v(t,Z_c) - \hat{U}_l(t)\right] + 2\pi R_i \int_0^{z_l} h_{w2l}\left[T_{wl}(t,z') - T_l(t)\right]dz' \\ + 2\pi \int_0^{R_i} h_{wh2l}\left[T_{wh}(t,r') - T_l(t,0)\right] r' dr' \end{aligned} \tag{2}$$

with the initial condition

$$\hat{U}_l(0) = \hat{U}_l(T_{l,0}) \tag{2a}$$

In our improved model, the liquid phase is stratified in *n* slices (each slice corresponding to one node) along the vertical axis of the cylinder.

There are some additional assumptions made in the improved model. The first assumption is that the density of the liquid phase is taken as the average density in all the nodes (corresponding to a slices) in the liquid that will be used to determine the height of liquid in the cylinder. The second assumption is that the temperature at the bottom of the cylinder is taken to be the average of the temperature at all the nodes on the bottom heel.

For the bottom slice, the liquid energy balance equation will be as follows:

$$\begin{aligned} m_l(t)\frac{d\hat{U}_l(t)}{dt} = 2\pi R_i h_{w2l}\left[T_{wl}(t,z') - T_l(t)\right]dz + 2\pi \int_0^{R_i} h_{wh2l}\left[T_{wh}(t,r') - T_l(t,0)\right] r' dr' \\ + \pi R_i^{\,2} k_l \frac{\partial^2 T_l(t,z)}{\partial t^2} dz \end{aligned} \tag{2b}$$

and for the top slice, the liquid energy balance equation will be as follows:

$$\begin{aligned} m_l(t)\frac{d\hat{U}_l(t)}{dt} = \dot{m}(t)\left[\hat{H}_g(T_v(t,Z_c) - \hat{U}_l(t)\right] + 2\pi R_i h_{w2l}\left[T_{wl}(t,z) - T_l(t)\right]dz \\ + \pi R_i^{\,2} k_l \frac{\partial^2 T_l(t,z)}{\partial t^2} dz \end{aligned} \tag{2c}$$

For the internal slices, the liquid energy balance equation will then be:

$$m_l(t)\frac{d\hat{U}_l(t)}{dt} = 2\pi R_i \int_0^{z_l} h_{w2l}\left[T_{wl}(t,z') - T_l(t)\right]dz' + \pi R_i^{\,2} k_l \frac{\partial^2 T_l(t,z)}{\partial z^2} dz \tag{2d}$$

3. Energy balance on the cylinder wall adjacent to liquid:

$$\pi(R_o^2 - R_i^2)\rho_c c_c \frac{\partial T_{wl}(t,z)}{\partial t} = 2\pi R_o h_{a2w}\left[(T_\infty - T_{wl}(t,z)\right] - 2\pi R_i h_{w2l}\left[T_{wl}(t,z) - T_l(t,z)\right] + \pi\left(R_o{}^2 - R_i{}^2\right)k_c \frac{\partial^2 T_{wl}(t,z)}{\partial z^2} \tag{3}$$

with the initial and boundary conditions

$$T_{wl}(0,z) = T_{wl,0} \qquad z \le z_l \tag{3a}$$

$$\frac{\partial T_{wl}(t,0)}{\partial z} = 0 \qquad t \ge 0 \tag{3b}$$

$$T_{wl}(t,z_l) = T_{wv}(t,z_l) \qquad t \ge 0 \tag{3c}$$

4. Energy balance on the cylinder wall adjacent to vapor:

$$\pi(R_o^2 - R_i^2)\rho_c c_c \frac{\partial T_{wv}(t,z)}{\partial t} = 2\pi R_o h_{a2w}\left[(T_\infty - T_{wv}(t,z)\right] - 2\pi R_i h_{w2v}\left[T_{wv}(t,z) - T_v(t,z)\right] + \pi\left(R_o{}^2 - R_i{}^2\right)k_c \frac{\partial^2 T_{wv}(t,z)}{\partial z^2} \tag{4}$$

with the initial and boundary conditions

$$T_{wv}(0,z) = T_{wv,0} \qquad \mathrm{z} \ge z_l \tag{4a}$$

$$\frac{\partial T_{wv}(t,Z_c)}{\partial z} = 0 \qquad t \ge 0 \tag{4b}$$

$$T_{wv}(t,z_l) = T_{wl}(t,z_l) \qquad t \ge 0 \tag{4c}$$

5. Energy balance on the cylinder heel:

$$\rho_c c_c \frac{\partial T_{wh}(t,r)}{\partial t} = h_{wh2l}\left[T_{wh}(t,r) - T_l(t,0)\right] + \frac{k_c Z_h}{r}\frac{\partial}{\partial r}\left[r\frac{\partial T_{wh}(t,r)}{\partial t}\right] \tag{5}$$

with the initial and boundary conditions

$$T_{wh}(0,r) = T_{wh,0} \qquad r \ge 0 \tag{5a}$$

$$\frac{\partial T_{wh}(t,0)}{\partial r} = 0 \qquad t \ge 0 \tag{5b}$$

6. Vapor phase Energy balance:

$$\pi R_i{}^2 \rho_g c_p V \frac{\partial T_v(t,z)}{\partial z} = 2\pi R_i h_{w2v}\left[T_{wv}(t,z) - T_v(t,z)\right] \tag{6}$$

with the initial condition

$$T_v(0,z) = T_{v,0} \qquad z \ge z_l \tag{6a}$$

Solution Procedure

The governing equations as discussed above, are solved using the method of lines [Magerøy-97]. In the method of lines, the second derivatives terms are approximated using a second order finite difference scheme:

$$\frac{\partial^2 X(z)}{\partial z^2} = \frac{X(z+dz) - 2X(z) + X(z-dz)}{dz^2}$$

where *X(z)* is the variable evaluated at the position *z*, *dz* is the spatial discretization and *dt* is the temporal discretization. The discretization results in a system of ordinary differential equations (ODEs). All these differential equations are converted to the form $y_i' = f\left(y_i, T, ...\right)$. The system of differential equations is solved using the LSODE (Lawrence Livermore Ordinary Differential Equations) Solver. Details of this package are provided by Hindmarsh [Hindmarsh-83]. The initial state of the system is used to calculate the internal energy of the liquid. The initial height of the liquid ESG in the vessel is also determined by the initial mass of ESG, initial temperature and distribution of the mass between the liquid and vapor phases. The physical properties of the vessel material are considered constant, whereas the physical properties for the ESGs are taken to be temperature dependent. The heat transfer coefficients are calculated using the correlation for forced convection, found in standard engineering heat transfer textbooks [Holman-86], using the physical properties that are updated at each time step. A constant value of 5 $\left(\frac{W}{m^2 \cdot s}\right)$ is used for the external (from ambient to cylinder wall) heat transfer coefficient. The heat transfer coefficient from wall to liquid is modified to account for the enhanced heat transfer due to rapid vaporization and associated vigorous boiling. The expression used for this modification is:

$$h_{\text{int}} = A \exp\left(-\frac{\left(y - y_{\text{int}}\right)}{B}\right) \tag{9}$$

where A and B are constants. The constant A and B are fixed at the same values for all available ESGs in the model.

Once the liquid internal energy is updated for each slice, the liquid temperature, at each time step, is then solved using the Newton Raphson method. The pressure is finally determined by using the vapor pressure correlation.

Mixing model

The improved model does not include a fluid dynamic model, thus it does not model the motion of the liquid due to the boiling phenomenon or natural convection. The result of boiling phenomenon and natural convection is the mixing of the liquid in the cylinder/ton vessel. Although we do not have a fluid dynamic model coupled with the heat transfer model, we propose a simplified model that takes into account the mixing of the liquid in the cylinder/ton vessel. We only consider three possible regimes in the liquid phase: the liquid would be either fully mixed, partially mixed, or locally mixed, which is a limiting case of partial mixing. As there could be a range of partial mixing regimes, accurate modeling of the partial mixing of the fluid could only be performed with a detailed model, such as a 2-D CFD model, capable of

capturing the motion of fluid in the cylinder/ton vessel. The main shortcoming for not having a fluid dynamic model is that we will need to use some empirical parameters to characterize the mixing of the liquid.

In order to determine the mixing regime in the liquid phase, we will use the Grashoff number, as follows:

$$Gr = \frac{\beta g L^3 \rho_{liq}{}^2 \Delta T}{\mu^2}$$

where β is the coefficient of thermal expansion of the liquid phase and μ is the viscosity of the liquid phase. The Grashoff number is characteristic of the natural convection. However, in order to have the Grashoff number account for the boiling phenomenon occurring in the cylinder we define the temperature difference ΔT as the difference of temperature resulting from the heat loss due to vaporization.

Three regimes will be distinguished depending on the value of Grashoff number. If the Grashoff number is below 1×10^8 the regime will be considered in the locally mixing regime. If the Grashoff number is between 1×10^8 and 8×10^8 the regime will be considered as the partial mixing regime. If the Grashoff number is above 8×10^8, the regime will be considered as the full mixing regime. In the full mixing regime, the heat transfer through the cylinder wall and due to vaporization of the liquid will be distributed to all the liquid slices. In the partial mixing regime, the heat transfer through the cylinder wall and the liquid vaporization will be spread out evenly to the top third of liquid. In the locally mixed regime, energy will be distributed only to the slices that are within 2 cm of the liquid-gas interface. When the liquid level is below 2 cm, the whole liquid phase in the cylinder will be considered at a uniform temperature. The cut-off values for the Grashoff number as well as the depth of the liquid affected by the mixing as used in our model were determined by a thorough analysis of all the experimental data available to us. These values are for ESG withdrawal from cylinders and may change for bulk systems or for other geometries.

Results

The presented model for liquid phase stratification and mixing has been tested with a variety of high-pressure, medium pressure, and low-pressure gases. The simulation of medium and high-pressure gases remains almost unchanged compared to the original model (no liquid stratification) because the mixing status is full mixing, therefore identical to the original model where the liquid was assumed to be at uniform temperature. In these experiments, the flow rates of such gases are high typically around 100 slpm.

Halocarbon 114 ($C_2Cl_2F_4$)

One trial with halocarbon 114 was run at Chicago Research Center (CRC). The initial mass of the liquid was 2.28 kg and the flow rate was 2.3 slpm (see Figure 2). The vessel used was a 7L carbon steel cylinder. The results with the modified model are slightly underpredicting the pressure in the cylinder with time. For this case, where the gas Halo 114 was low pressure and the withdrawal flowrate was low 2.3 slpm the simulation results were greatly improved.

Halocarbon 21 ($CHClF_4$)

There were two experimental runs with halocarbon 21 conducted at CRC. The cylinder used was a 7L aluminum cylinder. In the first run, the initial mass was 2.8 kg and the flowrate was 1.5 slpm (see Figure 3). The comparison between experimental and modified model simulation results shows that there is a very good agreement between the two. Again the modifications to the model helped to better predict pressure drop for a low pressure gas in this case Halo 21 at a low withdrawal flowrate of 1.5 slpm. There are spikes in the experimental results are because of intermittent mixing. During mixing the temperature of the liquid becomes more uniform, instead of having a top layer of cool liquid, therefore the pressure increases. When there is intermittent mixing, the pressure is closer to the pressure predicted by the original model. It is consistent with the fact that in the original model, the liquid is considered at uniform temperature, meaning that there is full mixing of the liquid in the cylinder. It can be noticed that as soon as the mixing stops, there is a large drop in pressure. This shows how the non-thermal equilibrium state of liquid can affect the pressure.

In the second run, at an initial mass of 2 kg and a flow rate of 3.36 slpm, the comparison between the experimental and simulation results shows that the pressure was slightly underpredicted in simulation (see Figure 4). The modified model simulation shows an improved pressure drop prediction, which more closely matched the general shape of the experimental pressure drop curve.

C_3F_8

There were many runs at various flowrates with C_3F_8 at CRC. For runs with large initial masses of liquid, the cylinder used was a carbon steel cylinder of size 44L. The masses used were 21 kg and 17.3 kg both at 10 slpm (see Figure 5 and Figure 6, respectively). The comparison of experimental data to the modified and original model simulation results shows good agreement. This could be explained by the flowrate of 10 slpm being sufficient to afford thorough mixing of the liquid. The modifications again do not affect cases where there is already good modeling of pressure drop. For runs with low initial masses of liquid, the cylinder used was an aluminum cylinder of size 7L. There were two runs with low initial mass, 4.5 kg, and flowrates of 3 slpm (see Figure 7) and 1 to10 slpm (see Figure 8). The results show that the simulation results using the modified model match well with the experiments while differing from the results of the original model. This clearly indicates that for a medium pressure gas at low flowrates the assumption of uniform liquid temperature is not valid.

Conclusions

An improved model has been developed to predict the pressure drop associated with withdrawal of ESGs from a cylinder or a bulk delivery system. The major change is in the treatment of liquid phase temperature, where the assumption of a uniform liquid temperature has been relaxed. In addition, an empirical mixing model is proposed that governs the extent of liquid depth affected by the energy loss due to vaporization of the liquefied ESG. This new model shows significant improvement for the prediction of pressure drop for medium-pressure and low-

pressure gases, although the mixing model is very simple and does not incorporate a fluid dynamic model. Inclusion of a 2-D CFD model may further improve the accuracy of the model and is the focus of ongoing work.

Nomenclature

A	Constant
B	Constant
c	Heat capacity, $J/(kg \cdot K)$
h	Heat transfer coefficient, $J/(kg \cdot m^2 \cdot K)$
H	Enthalpy, $J/(kg)$
i	Node index
k	Thermal conductivity, $J/(kg \cdot m \cdot K)$
L	Effective length of vessel, m
m	Mass, kg
N	Number of nodes
r	Radial coordinate, m
R	Radius, m
t	Time, s
T	Temperature, K
U	Internal Energy, J/kg
V	Velocity, m/s
z	z-axis coordinate, m
Z	height, m
Greek	
β	Coefficient of thermal expansion, $1/K$
ρ	Density, kg/m^3
μ	Dynamic viscosity, $kg/m \cdot s$
Subscripts	
$a2w$	External, ambient to wall
0	Initial
c	Cylinder
g	Gas
i	Inside
∞	Ambient
h	Heel
int	Interface

l	Liquid
liq	Liquid
m	Mean
o	Outside
v	Vapor
wh2l	Inside, bottom heel to liquid
wh	Bottom heel, liquid side
wl	Wall, liquid side
wv	Wall, vapor side
w2l	Inside, wall to liquid
w2v	Inside, wall to vapor

References

[Jurcik-96] Jurcik B., "A Model for Heat Transfer to a cylinder Containing a Gas Stored Under its Own Vapor Pressure," Internal Report, American Air Liquide, Chicago Research Center, (1996).

[Hindmarsch-83] Hindmarsh A. C., "ODEPACK, A Systemized collection of ODE Solvers," in Scientific Computing, (R. S. Stepleman, editor), Vol. 1, p. 55, IMACS Transactions on Scientific Computation, North Holland, Amsterdam, (1983).

[Holman-86] Holman J. P., "Heat Transfer," Sixth Edition, McGraw-Hill Book Company, New York, (1986).

[Mageroy-97] Mageroy E., "Numerical Integration of Systems Arising from the Method of Lines," Department of Mathematical Sciences, The Norwegian University of Science and Technology, (1997).

[Wang-97] Wang H-C, Udischas R. and Jurcik B., "All Vapor Phase delivery of electronic specialty gases". Proceedings of SEMICON West '97 Gas Distribution Workshop, San Francisco, CA.

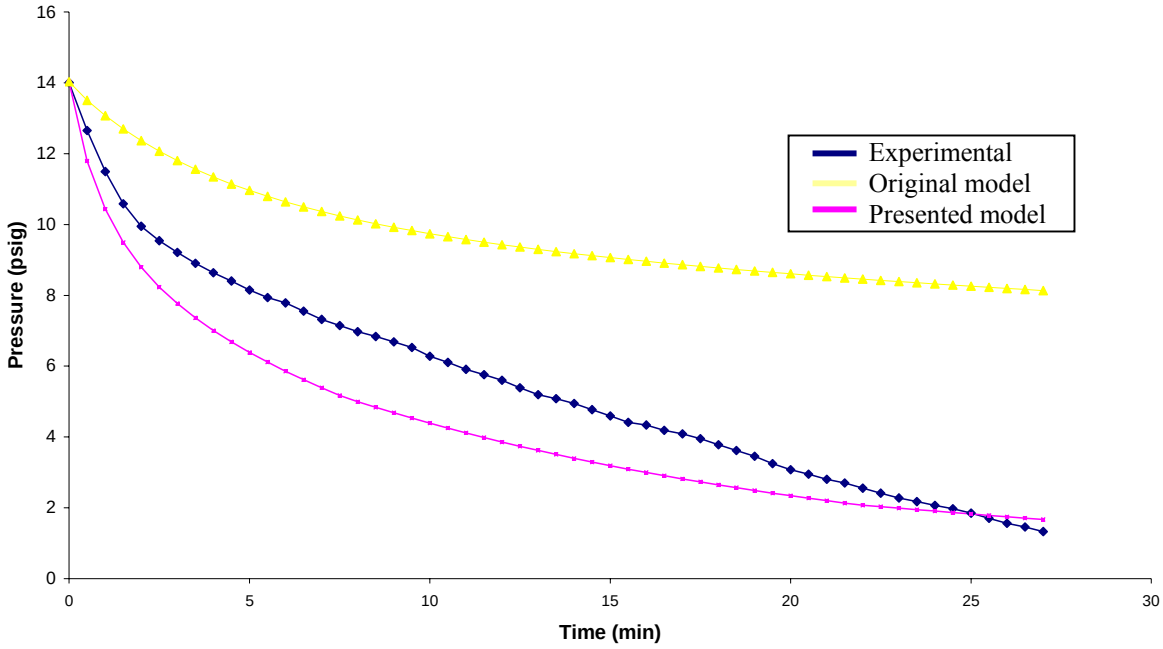

Figure 2. Pressure drop of 2.3 kg of Halo 114
(flow=2.3slpm, liquid height=8.5 cm, cylinder CS 7L)

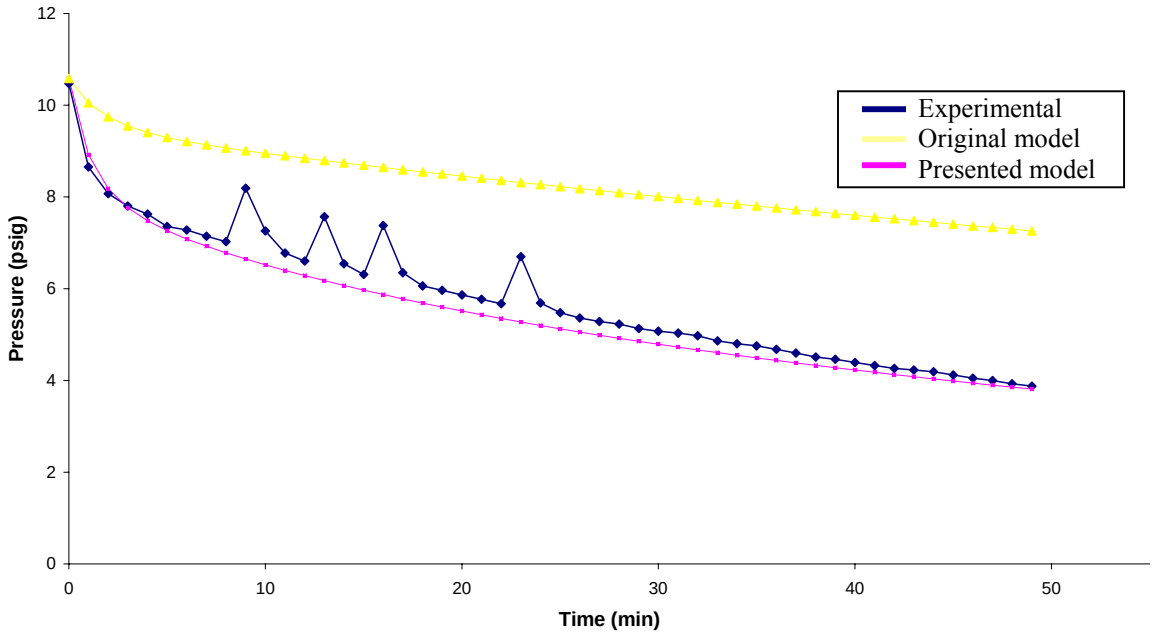

Figure 3. Pressure drop of 2.8 kg of Halo 21 with intermittent mixing
(flow=1.5 slpm, liquid height=10.5 cm, cylinder AL 7L)

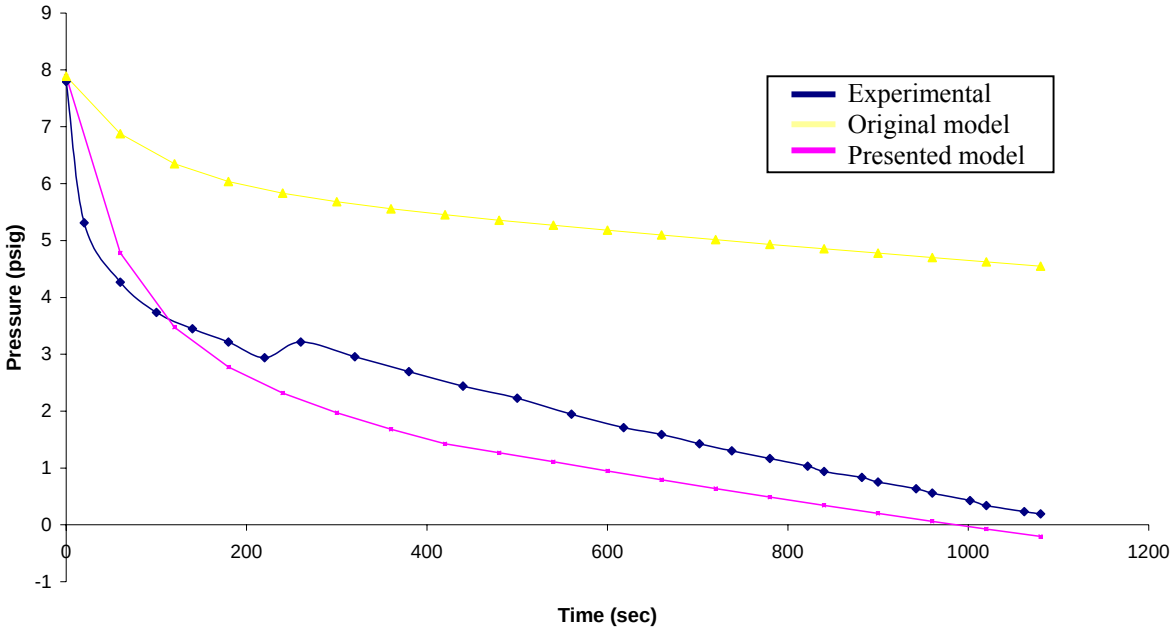

Figure 4. Pressure drop of 2kg of Halo 21
(flow=3.36 slpm, liquid height=7.5 cm, cylinder AL 7L)

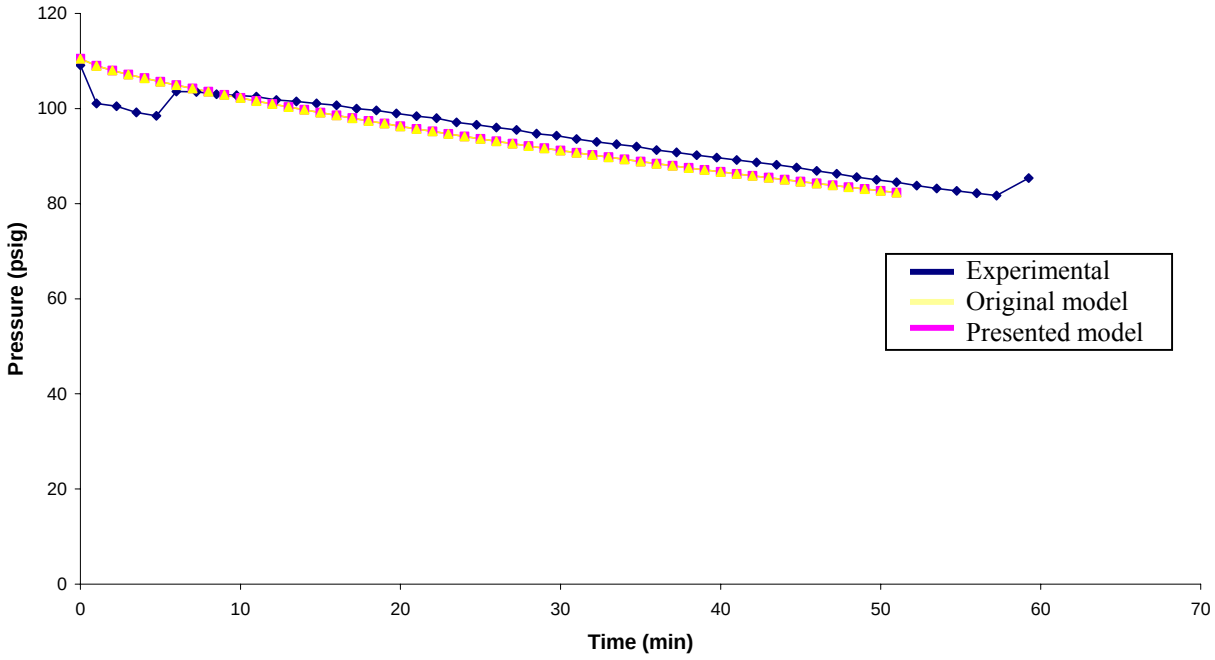

Figure 5. Pressure drop of 21 kg of C_3F_8 (flow=10 slpm, liquid height= 39.8cm,
cylinder CS 44L)

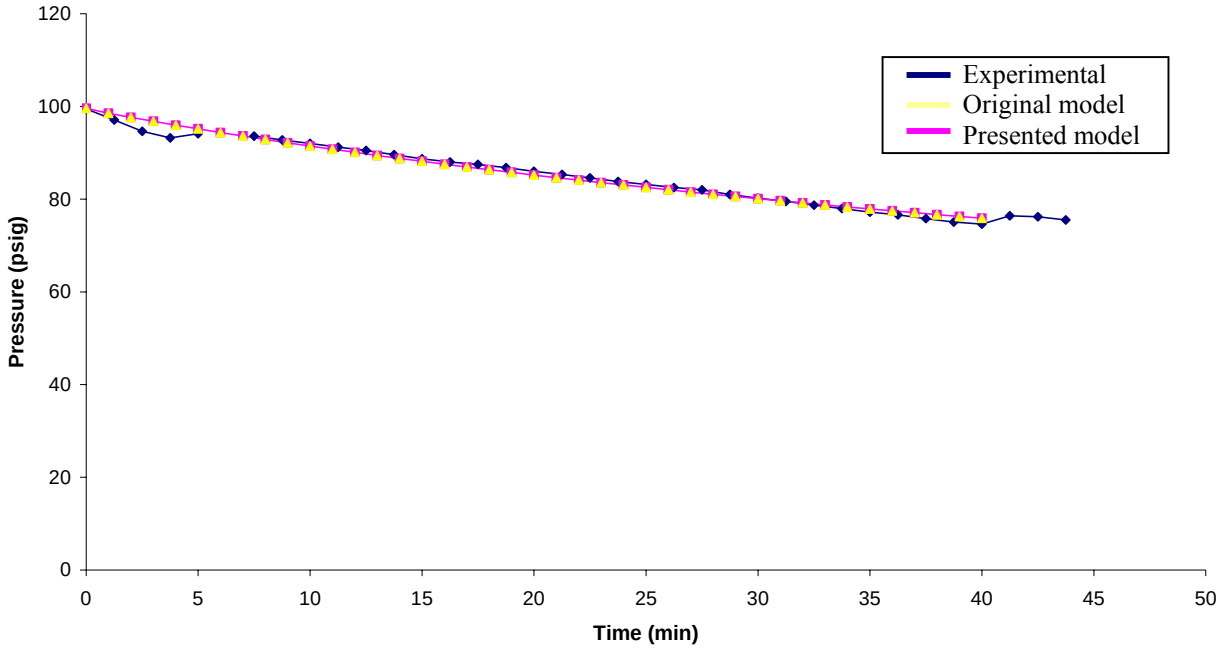

Figure 6. Pressure drop of 17.3 kg of C_3F_8 (flow=10 slpm, liquid height=30.8 cm, cylinder CS 44L)

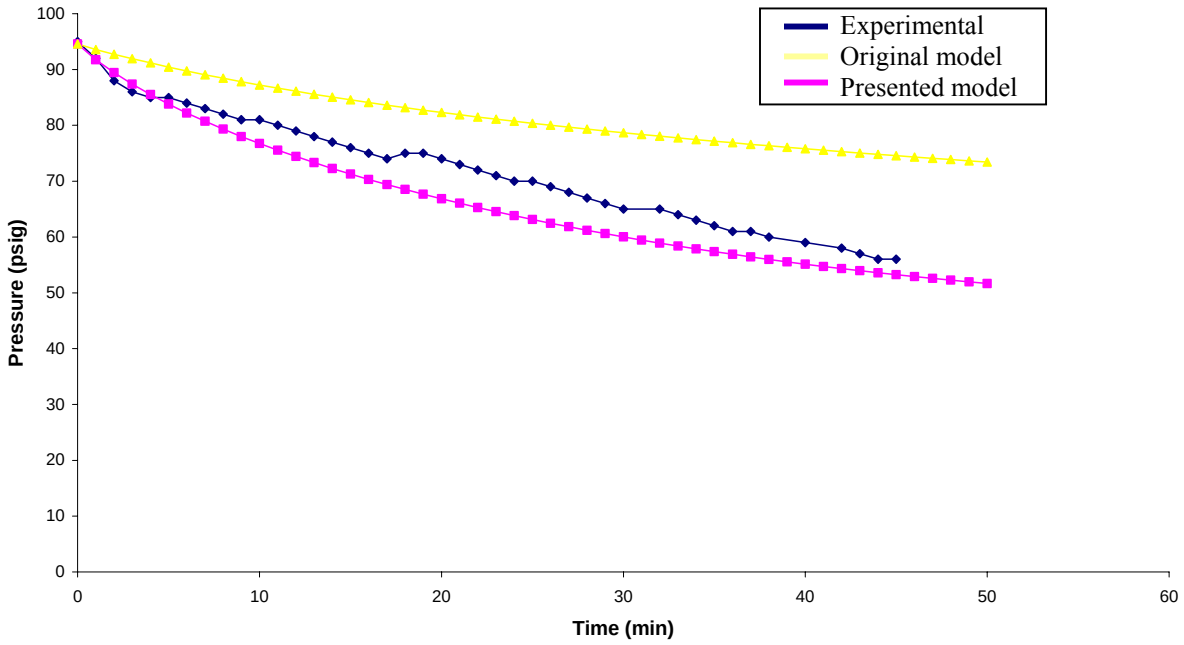

Figure 7. Pressure drop of 4.5 kg of C_3F_8 (flow=3 slpm, liquid height=16.9 cm, cylinder AL 7L)

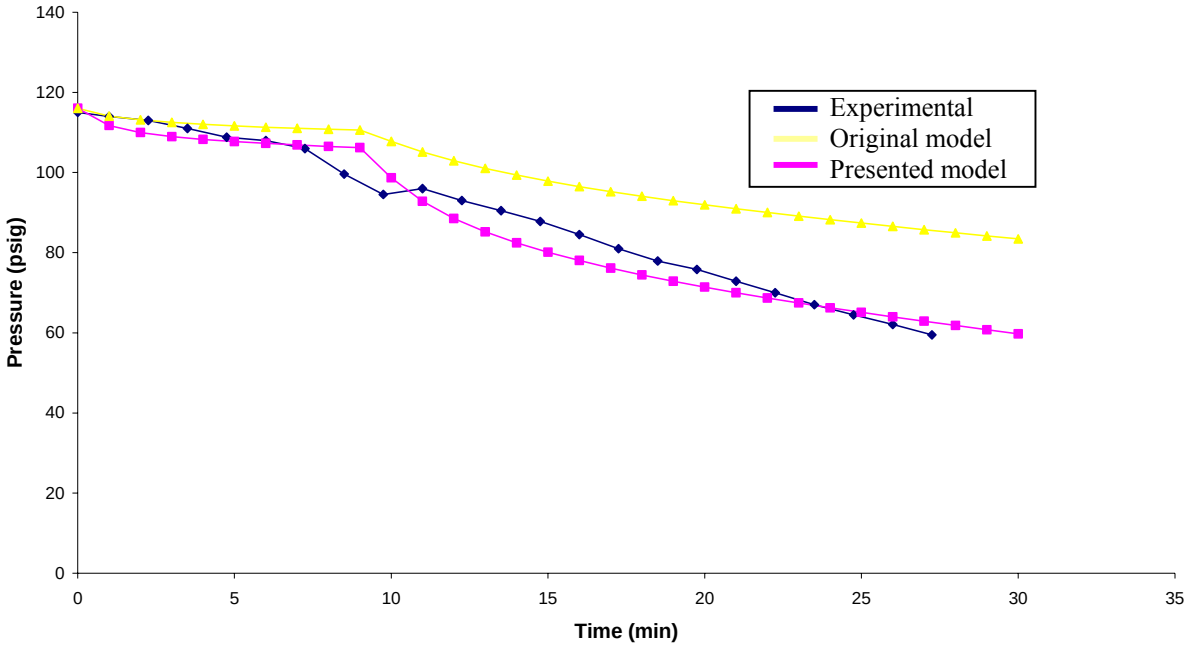

Figure 8. Pressure drop of 4.5 kg of C_3F_8 (flow=1-10slpm, liquid height=16.9 cm, cylinder AL 7L)